Coarse-Grained Simulations of Rapid Assembly Kinetics for Polystyrene-*b*-poly(ethylene oxide) Copolymers in Aqueous Solutions

Ting Chen, Antti-Pekka Hynninen, Robert K. Prud'homme, Ioannis G. Kevrekidis, and Athanassios Z. Panagiotopoulos*

Department of Chemical Engineering, Princeton University, Princeton, New Jersey 08544-5263

Received: July 2, 2008; Revised Manuscript Received: September 10, 2008

We present a coarse-grained, implicit solvent model for polystyrene-*b*-poly(ethylene oxide) in aqueous solution and study its assembly kinetics using Brownian dynamics simulations. The polymer is modeled as a chain of freely jointed beads interacting through effective potentials. Coarse-grained force field parameters are determined by matching experimental thermodynamic quantities including radius of gyration, second virial coefficient, aggregation number, and critical micelle concentration. We investigate the influence of cooling rate (analogous to the rate of solvent quality change in rapid precipitations), polymer concentration, and friction coefficient on the assembly kinetics and compare simulation results to flash nanoprecipitation experiments. We find that assembly kinetics show a linear scaling relation with inverse friction coefficient when the friction coefficient is larger than 1. When the cooling time is less than the characteristic micellization time, stable kinetically arrested clusters are obtained; otherwise, close-to-equilibrium micelles are formed. The characteristic micellization time is estimated to be only 3−6 ms, in contrast to 30−40 ms previously determined in experiments. We suggest that previous experiments probed the formation of micellar clusters while simulations in this work studied the kinetics of a single micelle assembled from free polymer chains.

1. Introduction

Self-assembly of block copolymers in aqueous solutions has been studied extensively through theory, experiment, and simulation due to its many industrial and pharmaceutical applications. Recently, diblock copolymers were used as size controlling agents in the flash nanoprecipitation process, a new technique for obtaining nanoparticles with narrow size distributions.[1−3] In this process, diblock copolymers and organic solutes (e.g., hydrophobic drugs) are first dissolved in an organic solvent (such as tetrahydrofuran) and are then quickly mixed with antisolvent (e.g., water) in a specially designed vortex micromixer to allow the fast precipitation of organic solutes and block copolymers. In a conventional direct precipitation processes, it is difficult to control the size of aggregates. In the flash nanoprecipitation process, diblock copolymers form a protective hydrophilic layer on the surface of the growing nanoparticles, which effectively arrests their growth. This rapid assembly process results in nanoparticles with low polydispersity and controllable mean particle size between 50 and 300 nm, a range desirable for applications such as drug delivery and cancer therapy.[4] The mechanism of block copolymer assembly in the flash nanoprecipitation process has been studied experimentally.[1,5] It was found that copolymers of low critical micelle concentration and fast mixing lead to homogeneous precipitation kinetics, where the size of nanoparticles is independent of initial polymer concentration and mixing rate. However, a microscopic understanding of assembly kinetics is still missing. In order to achieve that goal, it is crucial to first obtain a reliable, physically relevant model for the block copolymer.

Atomistic simulations are not computationally feasible for complex systems that span multiple time and length scales. To overcome this problem, various coarse-grained (CG) methods have been developed and extensively explored recently.[6−17] These methods work by grouping several atoms, or even an entire molecule like a polymer chain, into a single bead (sometimes called a blob), where chemical and physical details on finer levels are ignored or treated in a mean-field manner. Depending on the coarse-graining level, simulations based on such models can achieve several orders of magnitude increase in the time and length scales they can reach, as compared to fully atomistic simulations. Furthermore, implicit solvent models can be used to achieve significantly accelerated kinetics since one no longer needs to simulate solvent molecules. In this case, solvent effects are either totally neglected or approximated, for example, by incorporating an effective drag in the simulation. Simulations using CG methods have been reported in the literature for a wide variety of problems including polymer melts,[11,12,18] micelle formation of diblock copolymers,[7,10] and biomolecular membranes.[9,19]

Examples of recently proposed systematic methods for obtaining CG potentials include reverse Monte Carlo[20,21] or iterative Boltzmann inversion[22] where the effective potentials in CG simulations are tuned to reproduce structural distributions such as the inter- and intramolecular radial distribution functions (RDF) from reference atomistic simulations. Certain experimental quantities such as the bulk density and surface tension can also be used in the parametrization.[7,23] The effective potentials contain entropic contributions and thus are concentration and temperature dependent. Izvekov et al. recently developed a systematic approach of deriving CG force fields by matching the trajectories and forces in reference atomistic simulations with corresponding CG simulation data.[8,9] Noid et al.[24,25] proposed a systematic variation approach that can determine CG force field parameters via a least-squares approach from atomistic simulation data. While rigorous and useful, such CG methods provide moderate improvements in the effective time and length scales that CG simulations can access, and there

* Corresponding author. E-mail: azp@princeton.edu.

10.1021/jp805826a CCC: $40.75 © 2008 American Chemical Society
Published on Web 11/19/2008

is also no guarantee that such CG simulations can reproduce thermodynamic properties (e.g., solubilities or critical micelle concentrations) not included explicitly in the parametrization.

In this work, we demonstrate an ad hoc CG modeling approach for block copolymer assembly using pertinent experimental properties and study its self-assembly kinetics. We chose polystyrene-*b*-poly(ethylene oxide)—abbreviated as PS−PEO—as the model system since a significant body of experimental data exists on the physical chemistry and assembly kinetics of the micelles.[26,27] Our focus is on developing a CG model that is simple enough to allow efficient simulation, while still able to reproduce the thermodynamic properties of the target system. The main purpose of this work is to provide a foundation to better understand the fast assembly kinetics in the flash nanoprecipitation process, rather than developing a systematic coarse-graining methodology.

The paper is organized as follows. First, we explain how we choose the model, briefly describe the methods used in this work, and rationalize our choices. Then we show how we parametrize the CG force fields based on available experimental thermodynamic information. Next, we demonstrate how we determine the relevant time scales in the simulations compared to the actual experimental time scales. After that, we present simulation results on the rapid assembly of PS−PEO aqueous solutions and analyze the effect of cooling rate, or rate of solvent quality change, polymer concentration, and friction coefficient on assembly kinetics. The simulation results are discussed, when possible, within the context of relevant experimental observations.

2. Model and Methods

2.1. Explicit Solvent vs Implicit Solvent Model: A Time Scale Challenge. The rapid assembly of diblock copolymers in aqueous solutions in the flash nanoprecipitation process has the following features that are relevant and also challenging for CG modeling and simulation: (1) A mixing time of 2−20 ms.[28] (2) Assembly in dilute solution leads to polymer nanoparticles with sizes of 20−50 nm[1,2] and polymer−hydrophobic solute (β-carotene or gold nanoparticles) composite nanoparticles with sizes of 80−250 nm.[3] (3) Fast mixing of organic solvent with water and the use of polymers with low critical micelle concentration (cmc) result in a high rate of change of solvent quality: $dS/dt \sim 10^5\ s^{-1}$ where S is supersaturation and defined as the polymer concentration/C_{cmc}. This in turn provides a strong hydrophobic driving force for block copolymer assembly and produces kinetically arrested, nonequilibrium structures.

Features 1 and 2 essentially prohibit the use of a fully atomistic simulation method. Polymer concentration in experiments is usually less than 1 wt %, so an explicit solvent simulation would spend most of its time simulating the solvent dynamics, which is not of interest. An implicit solvent model is the only feasible approach. However, neglect of hydrodynamics makes implicit solvent simulations unable to reproduce certain features of the dynamic behavior of polymer solutions. For example, the diffusion coefficients of polymers in a dilute solution should obey Zimm theory,[29] $D \sim N^{-3/5}$, where N is the chain length, but implicit solvent simulations produce Rouse-type diffusive behavior[30] instead, $D \sim N^{-1}$.

Feature 3 requires us to use a dynamic method since we are trying to study the formation of nonequilibrium structures and relevant assembly kinetics. We emphasize that CG potentials are parametrized using selected equilibrium experimental observables, and then we perform dynamic simulations based on such a CG model.

Comparing with Noid et al.'s systematic variation approach,[24,25] our approach here is ad hoc and is designed specifically for better understanding of the flash nanoprecipitation process. While Noid et al.'s approach is more rigorous and provides an optimum approximation to the many-body potential of mean force in reference atomistic simulations, a more complicated potential brings also more restriction on the applicability of CG potentials as well as a moderate increase in the time scales the simulations can access. Considering the millisecond time scale of the flash nanoprecipitation process and our limited computational resources, we conclude that only an implicit solvent, coarse-grained modeling approach is feasible for our specific purpose.

2.2. Simulation Methods. We used a variety of computational methods in this work, including canonical ensemble MC simulation with configurational bias,[31] histogram reweighting,[32,33] grand canonical ensemble Monte Carlo (GCMC)[10,34] in the derivation of CG potential parameters for PS−PEO aqueous solution as well as BD simulations using the LAMMPS software package[35] with appropriate modifications.

Histogram reweighting GCMC obtains free energy information by combining multiple histograms at different chemical potentials, μ, and temperatures, T. It can be used to predict thermodynamic properties from certain conditions to other conditions (e.g., different μ, T). Note μ is relative to the chemical potential of a reservoir of ideal chains with only bonded interactions. Additionally, histogram reweighting GCMC can unambiguously determine the cmc by observing the sharp transition of osmotic pressure as a function of concentration in simulation.[34]

BD simulations in implicit solvent were performed using the LAMMPS package[35] in the NVT ensemble. The equations of motion were integrated by a velocity-Verlet algorithm with a time step of 0.003τ, where τ is the unit time. How this unit time is related to real time and how the friction coefficient, as seen in the following equation, influences the determination of τ in real units are discussed in section 3.3. BD simulations are governed by the Langevin equation

$$m_i \ddot{r}_i = -\gamma v_i + F_i^C + F_i^R \quad (1)$$

where m_i is mass, r_i and v_i are position and velocity vectors, F_i^C is the conservative force due to the inter- or intramolecular potentials, F_i^R is a random force that satisfies the fluctuation dissipation theorem with zero mean,[36] and γ is a friction coefficient. Friction force and random force work together as a thermostat to control the temperature in the BD simulation. The friction coefficient γ is related to the viscosity of the solvent, $\gamma = 6\pi d\eta$, where d is the bead diameter and η is the viscosity. Note that if we use the actual water viscosity at room temperature, the friction coefficient (Stokes drag) will be too large (in this work ~440 in reduced units), making the BD simulation computationally too demanding. In this work, we use a friction coefficient value of $\gamma = 1$ (the unit of friction coefficient is $m\tau^{-1}$ where m and τ are the unit mass and unit time), unless otherwise noted. The influence of the friction coefficient on the diffusive dynamics in a good solvent and assembly kinetics in a bad solvent is discussed in sections 3.3 and 4.3, respectively.

It is worth pointing out that Brownian dynamics does not preserve momentum and also does not incorporate the long-range hydrodynamic interactions.[37] Although DPD may provide an alternative simulation approach, an expensive explicit solvent is required to accurately model the solvent hydrodynamics.[37]

TABLE 1: Summary of Simulation Parameters and Physical Properties of $PS_{1000}-PEO_{3000}$ in Water in Both Reduced and Real Units[a]

properties	units	reduced value	real value
unit length, σ	σ	1.0	1.82×10^{-9} m
unit mass, m	m	1.0	6.2272×10^{-25} kg or 375 Da
unit energy, ε_h	ε_h	1.0	5.144×10^{-21} J
unit time, τ_0	$\sigma(m/\varepsilon)^{1/2}$	1.0	0.02×10^{-9} s when $\gamma_0 = 165$
unit time, τ (or τ_1, the unit time when $\gamma = 1$)	$f\sigma(m/\varepsilon)^{1/2}$	1.0	3.3×10^{-9} s when $\gamma = 1$
temperature, T	ε_h/k_B	0.8	298 K
friction coefficient, γ_0	$m\tau_0^{-1}$	165	5.137×10^{-12} kg/s
friction coefficient, γ	$m\tau^{-1}$	1.0	1.887×10^{-16} kg/s
diffusion coefficient, D	σ^2/τ	0.0962	0.977×10^{-10} m^2/s
radius of gyration squared, S^2	σ^2	1.0	3.31×10^{-18} m^2
second virial coefficient, A_2	σ^3	14.13	8.52×10^{-26} m^3
critical micelle concentration	σ^{-3}	1.15×10^{-5}	1.27×10^{-5} g/mL
length of PEO block		8	68 monomers
mass of PEO CG bead, H	m	1.0	375 Da
size of PEO CG bead, H	σ	1.0	1.82×10^{-9} m
length of PS block		5	10 monomers
mass of PS CG bead, T	m	0.53333333	200 Da
size of PS CG bead, T	σ	0.4	0.73×10^{-9} m

[a] f is the acceleration factor, and for $\gamma = 1.0$, $f = 165$. N is the number of polymer chains. Water density used is 1000 kg/m^3.

All data analysis was performed using self-developed codes, and block averaging methods proposed by Flyvbjerg et al.[38] were used when applicable.

3. Derivation of Coarse-Grained Potential Parameters

Coarse-grained force field parametrization was done by matching selected equilibrium thermodynamic quantities in experiments with corresponding Monte Carlo simulation results. We list all important simulation parameters in reduced units and their corresponding values in real units, as well as pertinent physical properties of $PS_{1000}-PEO_{3000}$ used in the simulation in Table 1 and discuss the derivation of these quantities in the sections that follow.

3.1. Potential between Hydrophilic PEO CG Beads. Poly(ethylene oxide), or PEO, is a biocompatible polymer that is widely used in the pharmaceutical and medical industry. Water is a good solvent for PEO for all molecular weights at room temperature. Surprisingly, there is little CG modeling or simulation of PEO in aqueous solutions, except for some simulations of short PEO chains in water.[39−41] Other CG models for PEO are found in studies of micellization of triblock copolymers containing hydrophobic poly(propylene oxide) (PPO) and hydrophilic poly(ethylene oxide) (PEO) blocks, such as the multiscale modeling approaches by Bedrov et al.[42] and implicit solvent MD simulations by Anderson et al.[43] In this work we model a PEO chain as a series of freely jointed identical beads interacting through an effective repulsive interaction. The nonbonded interactions are obtained by reproducing appropriate experimental thermodynamic properties.

There is still some debate in the literature whether long PEO chains associate with each other via hydrogen bonding to form aggregates or not, though water is a very good solvent for PEO.[44,45] Since we are interested in describing PEO chains at large coarse-graining levels, we do not include association between PEO chains and the effective interactions between them are chosen to be purely repulsive. The complicated behavior of PEO in water is best addressed by detailed atomistic simulations, which are outside the scope of the present work.

The form of the repulsive potential as well as the corresponding size and energy parameters are determined by simultaneously matching simulation results to experimentally measured scaling laws for the radius of gyration and second virial coefficient. It has been shown[45] that the mean-square radius of gyration of PEO chains in water scales as $\langle S^2 \rangle = 4.08 \times 10^{-22} M_w^{1.16}$ m^2 while the second virial coefficient scales as $A_2 = 3.72 \times 10^{-3} M_w^{-0.19\pm0.02}$ m^3 mol/kg^2. The second virial coefficients reported in experiments can also be expressed in the units of molecular volume by multiplying the experimental data by M_w^2/N_A;[46] then the above second virial coefficient scaling law becomes $A_2 = 6.177 \times 10^{-33} M_w^{1.81\pm0.02}$ m^3.

Canonical ensemble (NVT) MC simulation with the configurational-bias method was used to calculate the effective pair potential $U(r)$ between two polymer chains where the second virial coefficient A_2 can be calculated by numerical integration of the Mayer f-function, $f(r) = \exp[-U(r)/(kT)] - 1$,[47] of $U(r)$ over all interchain distances:[48,49]

$$A_2 = -\frac{1}{2}\int f_{12}\, d\vec{r} = 2\pi \int_0^\infty r_{12}^2 (1 - \exp(-U_{12}(r_{12})/kT))\, dr_{12} \quad (2)$$

The potential of mean force between two chains is expressed as a function of the distance between their centers of mass. To do this, multiple independent configurations of two polymer chains were generated by considering only intramolecular interactions.

Different forms and strengths of repulsion for freely jointed chains lead to different scaling exponents of radius of gyration and second virial coefficient. We considered a few types of repulsive interactions with different interaction ranges at different temperatures, including hard sphere repulsion, 12−6, 9−6, 8−6, and 6−4 Lennard-Jones potentials cut and shifted at the potential minimum (thus repulsive), and Gaussian repulsion. Using the two experimentally determined scaling exponents as matching criteria, we determined the following cut and shifted Gaussian repulsion as the effective interaction between PEO CG beads:

$$U(r) = \varepsilon_h(\exp(-6r^2) + \exp(-6r_{hcut}^2)) \quad (3)$$

with a cutoff distance $r_{hcut} = 1.2\sigma$ at a reduced temperature of $T = 0.8(\varepsilon_h/k_B)$, where ε_h and σ are energy and size parameters and k_B is the Boltzmann factor. A reduced temperature value of $T = 0.8(\varepsilon_h/k_B)$ can be used to calibrate the energy parameter ε_h, since reference experiments were performed at room temperature, and thus $\varepsilon_h = k_B T_{room}/0.8 = 5.144 \times 10^{-21}$ J. This Gaussian repulsion can be written in a more familiar form $U(r) = \varepsilon_h \exp(-r^2/2d^2)$, where $d = (1/12)^{1/2}\sigma$ is the characteristic distance scale. A similar Gaussian model with a FENE bond potential for polymer chains has been studied before, and it was found that the model gives unrealistic dynamical behavior in the concentrated regime.[50] This should not be a problem in this work, since we are concerned with assembly dynamics from a dilute solution.

Using this particular Gaussian potential, we obtained a radius of gyration scaling exponent of 1.17, in excellent agreement with experimental observations. The scaling exponent of the second virial coefficient as a function of chain length is −0.23, as compared to −0.19 found in experiments.

On the other hand, when we try to match the two prefactors in simulated scaling relationships, $\langle S^2 \rangle = 0.126N^{1.17\pm0.02}\sigma^2$ and $A_2/N^2 = 0.244N^{-0.23\pm0.01}\sigma^3$, or $A_2 = 0.244N^{1.77\pm0.01}\sigma^3$, to corresponding experimental results, we find that the size parameter estimated from matching the radius of gyration scaling is always about twice as large as the size parameter estimated from matching the second virial coefficient scaling irrespective of what mapping ratio we use. We are not able to simultaneously match all four parameters (i.e., two exponents and two prefactors), so we choose to match three parameters as closely as possible and allow some deviation in the last parameter. Here we match the prefactor of the radius of gyration scaling law as well as the two scaling exponents to experimental results; the size parameter can thus be estimated when we decide what mapping ratio we want to use. This choice consequently results in second virial coefficients that are about 7 times higher in simulations than in experiments.

3.2. Potential between Hydrophobic PS CG Beads and PS−PEO CG Beads. The specific PS−PEO diblock copolymer considered in this work consists of a hydrophobic PS block that has a molecular weight of 1000 Da, or 10 PS monomers, and a hydrophilic PEO block that has a molecular weight of 3000 Da, or 68 PEO monomers. $PS_{1000}-PEO_{3000}$ forms micelles in water that have an aggregation number $N_{agg} = 41$; these experiments were performed at a concentration of 5−10 g/L by Bronstein et al.[26] A critical micelle concentration (cmc) of 1.27×10^{-3} wt % was measured for $PS_{1000}-PEO_{3000}$ in water by Mortensen et al. at room temperature. Here we used Mortensen et al.'s cmc result and Bronstein et al.'s aggregation number measurement in our parametrization.

In Bronstein et al.'s work, it was found that the micelle size distribution of $PS_{1000}-PEO_{3000}$ in water exhibits two peaks: one corresponds to single micelles of $M_w = 2.55 \times 10^5$, and the other corresponds to secondary micellar clusters of $M_w = 2.8 \times 10^6$. They also measured the effective molecular weight of a single PS−PEO chain in THF as 6200. The single micelle thus has an aggregation number of 41, and the secondary micellar cluster has an apparent aggregation number of 452. The latter was in agreement with Mortensen et al.'s measurement on the aggregation number of the same PS−PEO system, 470, indicating that what Mortensen et al. observed is actually micellar clusters instead of single micelles. It was argued that hydrogen bonding between PEO units and between PEO unit and water may be responsible for the formation of micellar clusters.[26] Bronstein et al. observed the suppression of micellar clusters by adding some salts in an attempt to reduce the possibility of hydrogen-bonding interactions,[26] which seems to support this explanation.

Experiments usually use a mixture of THF and water, where THF to water volume ratio varies between 1:1 and 1:9. It has been shown that the cmc of $PS_{1000}-PEO_{3000}$ in a THF/water mixture increases as water content increases, but at a 1:1 THF to water content, $PS_{1000}-PEO_{3000}$'s cmc[51] is basically the same as in pure water,[26] about 10^{-3} wt %. So here we just use $PS_{1000}-PEO_{3000}$'s cmc in pure water.

The choice of mapping ratio is rather arbitrary, and this is also true in the literature. We choose a 8.5:1 mapping ratio for the PEO block, so that 68 PEO monomers can be represented by 8 CG beads, each of which has a unit weight of $m = 375$ Da, and the diameter of PEO CG bead σ is estimated as 1.82 nm (when matching the prefactor of radius of gyration scaling law to experimental value after the conversion of all reduced units to SI units). Meanwhile, we choose a 2:1 mapping for the PS block, so that 10 PS monomers are modeled by 5 PS CG beads. For convenience, we also denote a hydrophobic PS CG bead as a tail group (T) and a hydrophilic PEO CG bead as a head group (H). As such, the $PS_{1000}-PEO_{3000}$ diblock copolymer can be modeled by a CG model denoted as H_8T_5. Thirteen CG beads are tangentially connected with fixed bond lengths of σ, σ_t, and σ_{ht}, where σ is the bond length between head groups, σ_t is the bond length between tail groups, and σ_{ht} is the bond length between head and tail group and is calculated as the arithmetic mean of σ and σ_t.

For hydrophobic interactions between tail groups (PS−PS), we chose a 9−6 cut-and-shifted Lennard-Jones (LJ) potential:

$$U_{tt}(r) = \frac{27}{4}\varepsilon_t\left[\left(\frac{\sigma_t}{r}\right)^9 - \left(\frac{\sigma_t}{r}\right)^6 - \left(\frac{\sigma_t}{r_{tcut}}\right)^9 + \left(\frac{\sigma_t}{r_{tcut}}\right)^6\right] \quad (4)$$

where $r_{tcut} = 2(3/2)^{1/3}\sigma_t$ is the cutoff distance and ε_t is the energy parameter for tail−tail interaction. Choosing 9−6 instead of 12−6 LJ potential takes into account the soft nature of the CG PS bead as compared to the regular PS monomer.

The interaction between head and tail (PS−PEO) is difficult to prescribe since the relevant experimental information is lacking. We tried two types of potentials: Gaussian repulsion, similar to eq 3, where $r_{htcut} = 1.2\sigma_{ht}$, $\sigma_{ht} = (\sigma + \sigma_t)/2$, and ε_{ht} are the cutoff distance, size parameter, and energy parameter for the head−tail interaction, respectively, and a 9−6 Weeks−Chandler−Andersen (WCA) type of potential (i.e., 9−6 LJ potential cut and shifted at the potential minimum)

$$U_{ht(r)} = \frac{27}{4}\varepsilon_{ht}\left[\left(\frac{\sigma_{ht}}{r}\right)^9 - \left(\frac{\sigma_{ht}}{r}\right)^6 - \left(\frac{\sigma_{ht}}{r_{htcut}}\right)^9 + \left(\frac{\sigma_{ht}}{r_{htcut}}\right)^6\right] = \frac{27}{4}\varepsilon_{ht}\left[\left(\frac{\sigma_{ht}}{r}\right)^9 - \left(\frac{\sigma_{ht}}{r}\right)^6\right] + \varepsilon_{ht} \quad (5)$$

where $r_{htcut} = (3/2)^{1/3}\sigma_{ht}$, $\sigma_{ht} = (\sigma + \sigma_t)/2$, and ε_{ht} are the cutoff distance, size parameter, and energy parameter for the head−tail interaction, respectively. Note that the key difference between tail−tail (eq 4) and tail−head potentials (eq 5) is the cutoff distance, which makes tail−head interactions repulsive at all distances.

We found that large, ill-formed micelles with an aggregation number well over 100 appear when Gaussian repulsion was used

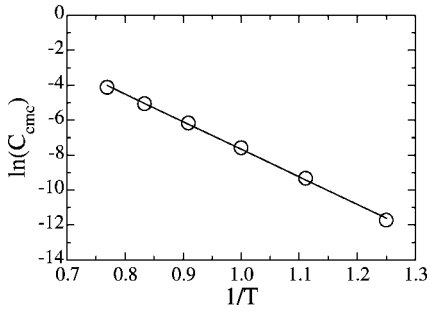

Figure 1. $\ln(C_{cmc})$ as a function of inverse temperature, $1/T$, for H_8T_5. $L = 15$, $T = 0.8$. The line is a linear fit of data.

as the effective interaction between the head and tail groups, as compared to the spherical micelle with an aggregation number of 41 found experimentally. Therefore, we decided to use the 9−6 WCA type of potential.

The core of PS−PEO micelles consists mainly of PS monomers and is meltlike.[27] On the basis of this information, we estimated the size of PS CG bead by matching the PS melt density 0.95 g/cm^3 to the dense random packing of LJ particles, 0.64;[52] we then obtain σ_t as 0.73 nm, or 0.4σ. The two remaining parameters, ε_t and ε_{ht}, were obtained by reproducing the experimentally observed cmc (mainly influenced by ε_t) and aggregation number (influenced by both ε_t and ε_{ht}) at $T = 0.8$ (designated as room temperature, 298 K).

We studied different combinations of ε_t and ε_{ht} using histogram reweighting grand canonical ensemble simulations. The simulations are performed at different temperatures in a $15\sigma \times 15\sigma \times 15\sigma$ box. The experimental cmc in terms of number of polymer chains per unit volume, C_{cmc}, is $1.15 \times 10^{-5}(\sigma^{-3})$ after unit conversion, or 1.27×10^{-3} wt % in real units. For $\varepsilon_t = 1.30$ and $\varepsilon_{ht} = 0.01$ the histogram reweighting calculation obtains a cmc of $0.9 \times 10^{-5}(\sigma^{-3})$, or 1×10^{-3} wt % in real units, where cmc is defined as the number density of copolymer at which a sharp transition in the osmotic pressure curve is observed.[34] The aggregation number is determined as 43, at thermodynamic conditions where histogram reweighting prediction and simulation results agree with each other, and the aggregation number decreases as T increases. We obtained C_{cmc} at different temperatures and found them to follow the relationship of $\ln(N_{cmc}) = A + B/T$,[34] as shown in Figure 1. This relationship could be useful if parametrization needs to be done for polymers with even lower cmc.

3.3. Diffusivity and Time Scale Mapping. So far we have obtained a CG model with appropriate potential parameters for $PS_{1000}-PEO_{3000}$ in water based on pertinent experimental thermodynamic quantities. The CG model and parameters derived in the previous section were used in LAMMPS simulation, except for one difference: in MC simulation, we used a freely jointed model and only the fixed bond length constraint is considered. However, LAMMPS limits the use of the SHAKE algorithm, frequently employed to restrain the bond length in molecular dynamics simulation, to only small clusters like water molecules. To mimic the fixed bond length constraint in MC simulations, we use a bead−spring model in LAMMPS simulation with a strong harmonic bond $E_{bond} = {}^1/_2k(r - r_0)^2$ constraining the bond length at $r_0 = 1\sigma$. For a harmonic bond constant of $k = 10\,000$, a Boltzmann distribution of bond lengths at $T = 0.8$ is a Gaussian function with a standard deviation of 0.009σ (i.e., $1 \pm 0.018\sigma$ at 95% confidence level). We found a 2% systematic difference between radius of gyrations calculated in LAMMPS MD and the corresponding MC results.

3.3.1. Calculation of the Diffusion Coefficient. In this section, we show how we related the time scales in BD simulations to the experimental time scales. This was done by matching simulated diffusion coefficients of CG PEO and PS−PEO chains in a good solvent to corresponding experimental measurements. In simulations, the diffusion coefficient is calculated via mean-square displacement (MSD), $D = (\langle[R_{cm}(t) - R_{cm}(t_0)]^2\rangle)/6t$, at long times, where MSD changes linearly as a function of simulation time. A multiple time origin average method[53] was used to improve the statistics in the calculation of diffusion coefficients. Note that momentum is not conserved in BD simulations and the system as a whole also diffuses, so the center of mass diffusion coefficient of the whole system was subtracted from that of the polymer chains.

We calculate the center of mass self-diffusion coefficients of PEO_{3000} (where 68 monomers are represented by 8 head groups) in a BD simulation with $\gamma = 1$. We then compare the computed diffusion coefficient value, $0.0953\sigma^2/\tau$, with the experimental measurement of self-diffusion coefficient extrapolated to infinite dilution for the equivalent PEO chains in water, $D_0 = 0.971 \times 10^{-10}$ m^2/s.[54] After units conversion, we find the time scale in simulation, $\tau = 3.3$ ns. The intrinsic time scale in current BD simulation can be computed by $\tau_0 = \sigma(m/\varepsilon)^{1/2}$, and we obtain $\tau_0 = 0.02$ ns, or 20 ps given $\sigma = 1.82 \times 10^{-9}$ m, $m = 375$ Da $= 6.2272 \times 10^{-25}$ kg, and $\varepsilon = 5.144 \times 10^{-21}$ J. So the extra "speed-up" factor due to the use of a weak friction coefficient of background solvent is about 165 times for BD at the simulation conditions.

Bronstein et al. measured the diffusion coefficient of $PS_{1000}-PEO_{3000}$ in THF (a good solvent) to be $D_0 = 1.25 \times 10^{-10}$ m^2/s. We computed the diffusion coefficient of H8T5 at $T = 1.5$, $D_0 = 1.254 \times 10^{-10}$ m^2/s using $\tau = 3.3$ ns, which matches well with the experimental diffusion coefficient of PS−PEO in THF. An initial simulation state at $T = 1.5$ can thus be compared with the starting good solvent condition for PS−PEO in the flash nanoprecipitation experiments.

Furthermore, we find that there is no appreciable finite size effect in the computation of diffusion coefficients. For the density dependence, the diffusion coefficient at low densities in BD simulations increases linearly by 1−2% as the density decreases from 1.3 to 0.16 wt %, similar to what has been reported in the literature.[54] The extrapolated diffusion coefficient at infinite dilution in a BD simulation when $\gamma = 1m\tau^{-1}$ is $0.0962\sigma^2/\tau$.

3.3.2. Molecular Weight Dependence. In experiments, different scaling laws of diffusivity as a function of molecular weight for PEO in water have been found. Shimada et al.[55] reported a −0.43 exponent for short chains with a molecular weight up to 1600, $D = (6.28 \pm 0.38) \times 10^{-9}M_w^{-0.43\pm0.01}$ m^2 s^{-1}, while Waggoner et al.[54] reported a scaling exponent of −0.6 but for a much broader molecular weight range. The Zimm model[29] predicts a scaling relationship of $D \sim N^{-0.59}$, and the Rouse model[30] predicts $D \sim N^{-1}$. It has been shown that solvent quality in a BD simulation does not change the $D \sim N^{-1}$ dependence for a model Gaussian chain,[50]and this is indeed what was observed (data not shown). Rouse-type behavior is a salient feature of the implicit solvent model, since implicit solvent corresponds to the situation where the hydrodynamic interaction is screened. We thus need to compute our time scale mapping again if a PS−PEO chain with a different molecular weight is used. An explicit solvent model should be used if Zimm type molecular weight dependence of the diffusion coefficient needs to be reproduced. A discrepancy in the scaling exponents between coarse-grained simulation and experiment is not

uncommon in the literature. For example, in CG modeling and simulation of *n*-alkanes, Nielsen et al. found the CG diffusion coefficients exhibiting a −1.35 scaling exponent in the $D \sim M_w$ scaling law where the experiment reported a −2.72 exponent.[56]

3.3.3. Influence of the Friction Coefficient. It is possible to adjust the friction coefficient to match the dynamics of a CG simulation with those of atomistic simulation.[11] Since the purpose of this work is to access a time scale on the order of milliseconds, it is desirable to use a small Langevin friction coefficient in order to enable simulation of longer time scales. The question now becomes: how does kinetics in the simulation scale with respect to the friction coefficient in BD simulations?

We have shown in previous sections that our implicit solvent simulations follow Rouse dynamics. For the Rouse model, all time-dependent properties scale on t/γ,[57] and Kindt et al.[12] have shown, for a polyethylene melt, that the dynamics in a BD simulation scale as a function of the factor $f = (\gamma^C + \gamma)/(\gamma^C + \gamma_0)$, where γ and γ_0 are friction coefficients used in BD simulations and γ^C is a kind of effective friction coefficient resulting from the pairwise potential between polymer chains. Accordingly, we should observe $D_\gamma/D_{\gamma_0} = (\gamma^C + \gamma_0)/(\gamma^C + \gamma)$, where D_γ is the diffusion coefficient at a friction coefficient of γ and D_{γ_0} is the diffusion coefficient at a friction coefficient of γ_0 for the same system. The ratio of D_γ/D_{γ_0} tells how much the simulation is accelerated or decelerated when a friction coefficient other than γ_0 is used. Indeed, our BD simulation showed that the diffusion coefficient of PEO chains in water scale linearly on the inverse friction coefficient, $D \sim \gamma^{-1}$, which requires $\gamma^C = 0$. This is a characteristic behavior of Rouse dynamics since $D = k_BT/\gamma N$[57] when the length of polymer chain does not exceed the entanglement length. The diffusion coefficient of PS−PEO at $T = 1.5$ (corresponding to the situation where PS−PEO is in a good solvent like THF) also scales linearly as a function of inverse friction coefficient. We thus demonstrated that the diffusive kinetics of PEO and PS−PEO in a good solvent have a simple scaling relation with the inverse friction coefficient, as predicted by the Rouse model. We will discuss how friction coefficient influences assembly kinetics of diblock copolymers in a bad solvent in section 4.3.

This linear dependence of diffusion coefficient on inverse friction coefficient suggests a friction coefficient of 165 should give us a unit time scale of 0.02 ns, consistent with the definition of the unit time, $\tau_0 = \sigma(m/\varepsilon)^{1/2}$, and introduce no extra acceleration effects in the BD simulation. In comparison, the time scale has been determined as 3.3 ns for a friction coefficient of 1. Even if we calculate an effective viscosity of the implicit solvent for $\gamma = 165m\tau^{-1}$or $\gamma = 165(m\varepsilon/o^2)^{1/2}$, we obtain $\eta = \gamma/6\pi d = 0.000147$ kg/(m s), which is less than the actual water viscosity at room temperature, 0.001 kg/(m s). This shows that in order to achieve the experimental diffusion coefficient, CG PEO chains need to move in a background solvent with about 1/7 of the actual solvent (water) viscosity. This is probably due to the 8.5:1 mapping ratio of PEO block.

4. Results and Discussion

4.1. Influence of Cooling Rate (Rate of Solvent Quality Change). In previous sections, we have chosen $T = 1.5$ as the starting state in the simulation, to represent the initial good solvent condition in the flash nanoprecipitation process, by matching the computed diffusion coefficient of PS_{1000}−PEO_{3000} at that temperature to its experimentally measured value. The final state in the simulation is $T = 0.8$, which corresponds to the bad solvent experimental condition at room temperature. In the experiment the solvent quality is changed by mixing organic solvent with water. In the simulation, this process is mimicked by gradually cooling the system from $T = 1.5$ to 0.8. Thus, the mixing time (or rate) in the flash nanoprecipitation experiment can be related to the cooling time (or rate) in the simulation. For the convenience of comparison, we do not distinguish mixing time and cooling time in the following discussion and refer to the time as a "quenching" time from good solvent to poor solvent. The quenching rates and times are expressed in real units assuming $\gamma = 1$ and $\tau = 3.3$ ns.

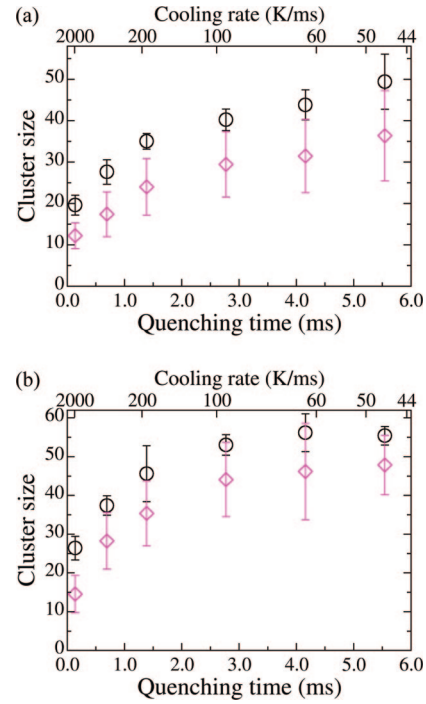

Figure 2. Size of the largest aggregate (circle) and average aggregation number (diamond) as a function of quenching time and rate. (a) $N = 250$, $L = 64$; (b) $N = 250$, $L = 44$. Data are averaged over five independent runs, and corresponding standard deviations are shown. Each symbol represents a different system: they are not from a single continuous simulation.

All simulations start from initial nonoverlapping states generated by a configuration-bias MC method and are equilibrated at $T = 1.5$ (558.75 K) for 10 million steps (equivalent to 0.099 ms), to make sure polymer chains are relaxed and randomly dispersed throughout the system. The system is then quenched slowly to $T = 0.8$ (298 K) in decrements of 0.05 in an NVT ensemble. The quenching rate varies from $\Delta T = -0.05$ per 1 million steps (1881 K/ms) to −0.05 per 40 million steps (47.03 K/ms). In the simulation, systems at three different densities are studied: 0.1, 0.3, and 0.6 wt %, and the total cooling time varies between 0.14 and 5.54 ms. Since the cmc of PS_{1000}−PEO_{3000} in pure water is 1.27×10^{-3} wt %, the supersaturation rate change in the simulation is of the order of 10^5−10^6/s, comparable to experimental conditions (about 10^5/s).[1] The cluster size distributions are analyzed at $T = 0.8$ over another 40−80 million steps after the cooling is performed. For the purpose of analyzing assembly kinetics, coordinates along each time evolution trajectory are stored at certain time intervals during the entire simulation.

Figure 2 shows the size of the largest aggregate and the average aggregation number as a function of quenching time and rate. In the calculation of average aggregation number we omitted the contribution from those small clusters with aggregation numbers less than 5. The polymer concentration is

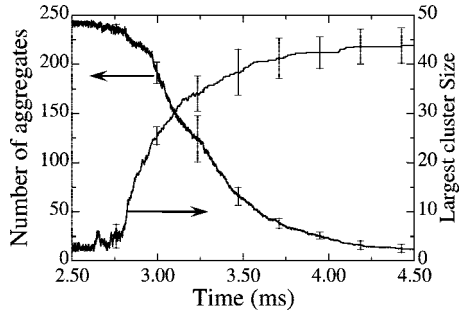

Figure 3. Evolution of the size of the largest aggregate and the number of aggregates as a function of simulation time. $N = 250$, $L = 64$, $\gamma = 1$. Data are averaged over five independent runs, and standard deviations are shown every 480 data points for clarity.

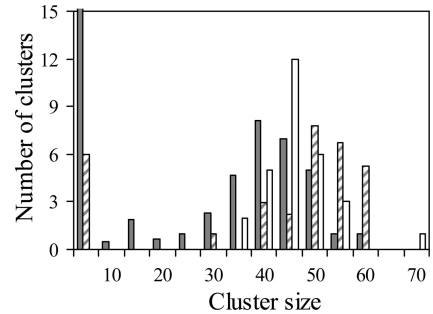

Figure 4. Cluster size distribution for $N = 250$, $L = 64$ (solid gray bars), 44 (striped bars) and 35 (white bars), corresponding to about 0.1, 0.3, and 0.6 wt % of polymer concentration when $\gamma = 1$. The employed quenching rate is 47.03 K/ms, corresponding to a total quenching time of 5.54 ms. Data are collected and accumulated from five independent runs and are binned into histograms with a width of 5.

0.0985 wt %. In the flash nanoprecipitation process, a large solvent quality jump in a short amount of time (or a small mixing time), combined with specifically tailored diblock copolymers with low critical micelle concentration, are key components to obtaining kinetically arrested structures with well-controlled size distributions. Once an overlapping brush on the particle surface is formed, the polymer nanoparticles should be stable in size. Indeed, we find that in the simulation faster quenching rates (corresponding to smaller mixing time in the experiment) lead to smaller, kinetically arrested, but stable aggregates. On the other hand, slower quenching rates (corresponding to larger mixing time in the experiment) lead to larger aggregates that are close to equilibrium structures. For the system shown in Figure 2a, both the size of the largest aggregate and the average aggregation number still evolve even at the largest quenching time investigated. However, at a higher density, as shown in Figure 2b, both the size of the largest aggregate and average aggregation number reach a plateau at around 3 ms (or when the quenching rate is slower than 94.2 K/ms). Further decreasing quenching rate (or equivalently increasing quenching time) does not increase the average aggregate number, indicating that equilibrium has been reached.

Because of kinetic trapping at low temperature, we cannot determine the exact equilibrium aggregation number in BD simulation. But we can judge if the system has reached, or at least is close to, the equilibrium state by monitoring how the system evolves following, for example, the time evolution of the number of aggregates, and the size of the largest aggregate. Additionally, we can also observe how the aggregation number changes as a function of quenching rate and if the aggregation number changes upon an extended simulation time. The fact that further decreasing quenching rate (corresponding to increasing mixing time in experiments), as shown in Figure 2, only slightly increases the size of the largest cluster in the presence of free chains in the simulation box suggests that the system has reached, or at least is very close to, equilibrium.

Figure 3 shows the evolution of the number of aggregates and the size of the largest aggregate with a quenching rate of 62.7 K/ms, or a total quenching time of 4.158 ms. Following the gradual quenching of the system, solvent quality becomes increasingly worse for tail groups (PS CG beads). Both curves feature a relatively sharp transition. No appreciable micellization occurs before 2.8 ms (corresponding to a temperature around 1.0), and before that time the trajectories are noisy due to constant fluctuation of the two properties monitored. After 4.2 ms (i.e., after the quenching is finished), micellization is complete, and both the number of aggregates and the size of the largest aggregate reach a plateau where the values of two properties are approximately constant. We observe the same trends for systems with faster quenching rates (smaller quenching time) where the size of the largest aggregate is smaller than the equilibrium aggregation number but still stable in size. Figures 2 and 3 together show that we can control aggregate size by controlling the quenching rate in the simulation (corresponding to controlling the mixing time in the experiment) since the rate of temperature drop (rate of solvent quality change) governs the assembly of polymer chains.

For all the systems, we observed that within a few milliseconds (~6 ms) clusters were formed with aggregation numbers varying between 35 and 65 (compared to the experimental aggregation number of 41 for $PS_{1000}-PEO_{3000}$), depending on the system density. This suggests that the characteristic micellization time scale for $PS_{1000}-PEO_{3000}$ in water should be less than 6 ms. This differs from the estimated characteristic aggregation time in the flash nanoprecipitation process,[1,2] which was 30−40 ms. Therefore, it is possible that the previously estimated characteristic aggregation time in the flash nanoprecipitation process actually corresponds to the characteristic time of association between nonequilibrium PS−PEO clusters since during fast quenching some "nonequilibrium" aggregates formed may have their hydrophobic core partially exposed, which may lead to their clustering. The micellar clusters may as well result from the clustering of PS−PEO micelles via hydrogen bonding between PEO blocks. In the experiment, the polymer nanoparticle size reaches a plateau of about 23 nm when the time of mixing the organic solvent with water is less than a characteristic aggregation time (e.g., 30 ms). This 23 nm polymer nanoparticle size is in excellent agreement with the hydrodynamic diameter of equilibrium micelles of $PS_{1000}-PEO_{3000}$, 25 nm, measured by Bronstein et al.[26] In contrast, we find in the simulation that when the quenching time is small (<3 ms, corresponding to a fast quenching rate), kinetically frozen aggregates are obtained in the simulation; and when the quenching time is large (>3 ms, corresponding to a slow quenching rate), clusters that are close to equilibrium structures are obtained. The time and length scales in the simulation and in the experiment overlap at equilibrium $PS_{1000}-PEO_{3000}$ micelle size of ~25 nm (or an aggregation number of 41) and a characteristic micellization time of about 6 ms. Our work thus provides a microscopic explanation of the phenomena occurring during the flash nanoprecipitation process and helps reconcile experimental observations.

4.2. Influence of Polymer Concentration. Figure 4 shows the cluster size distributions at polymer concentrations of 0.1, 0.3, and 0.6 wt % where labels on the *X* axis represent the upper limit of each size range. For example, 10 means a range of

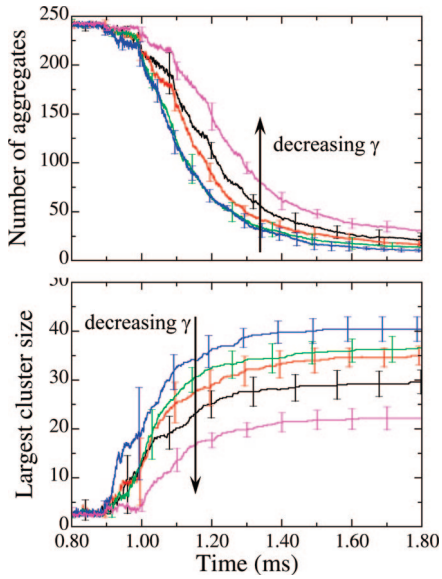

Figure 5. Number of aggregates in the system (upper plot) and size of the largest aggregate (lower plot) as a function of simulation time for different friction coefficients. $N = 250$, $L = 64$. $\gamma = 4.0$, 2.0, 1.0, 0.5, and 0.2 for curves from bottom to top in the upper plot and for curves from top to bottom in the lower plot. The effective quenching rate in all three simulations is 188.1 K/ms, and the corresponding total quenching time is 1.386 ms. Data are averaged over five independent runs, and standard deviations are shown every 200−400 data points for clarity.

aggregate sizes between 6 and 10; 20 means a range of aggregate sizes between 16 and 20. Average aggregation numbers at each concentration are 36.4 ± 10.9, 47.8 ± 7.6, and 43.1 ± 6.3, respectively. In the calculation of average aggregation number we omitted the contribution from those small clusters with aggregation numbers less than 5. We notice that in the simulation the average aggregation number first increases and then decreases as the polymer concentration increases. In order to make sure finite size effects are not causing this behavior we performed the simulation at 0.6 wt % concentration but with twice as many chains in a larger simulation box (500 chains in a cubic box of length 44). We obtained an average aggregation number of 43.8 ± 7.8, matching well with the average size of 43.1 ± 6.3 in a 250-chain system in a cubic box of length 35. As such, the finite size effect is minimal even at the highest polymer concentration, 0.6 wt %, and does not cause this nonmonotonic behavior of aggregation number on the concentration. The coarse-grained force field derived in this work is expected to lead to an equilibrium micelle with a most probable aggregation number of 43. As shown in Figure 4, the simulated most probable aggregation number at the investigated concentrations varies between 36 and 48 with rather broad distributions, bracketing the experimental value of 41[26] that was measured at densities between 0.5 and 1 wt %.

4.3. Influence of Friction Coefficient on Assembly Kinetics. In section 3.3.3, we have shown that the diffusion coefficients of PEO chains and PS−PEO chains in good solvent have a linear scaling relation with the inverse friction coefficient in the BD simulation, a typical behavior of Rouse dynamics. We now study whether the simulated assembly kinetics still lead to a similar simple scaling relation with the friction coefficient. This matters because we need to know if using an artificially smaller friction coefficient to accelerate simulation and reduce computational cost will alter the assembly kinetics.

Figure 5 shows the assembly trajectories from simulations with different friction coefficients. The time-dependent trajectories with nonunity friction coefficient are scaled by γ^{-1} and converted to real time units in ms in order to make comparison possible, i.e., $\tau_{0.2}:\tau_{0.5}:\tau_1:\tau_2:\tau_4 = 5:2:1:{}^1/_2:{}^1/_4$ (note that τ is determined by matching computed diffusion coefficients with experimental values; the larger the γ, the smaller τ is, and thus more time steps needed in order to reach the certain amount of real time).

As we can see in Figure 5, the time evolution of the number of aggregates in each system agrees well with each other when friction coefficients is greater than or equal to 2. The size of the largest aggregate in the system, however, increases as the friction coefficient increases when the systems with different friction coefficients are simulated for the same length in real time. Simulations with larger friction coefficient micellize earlier, manifested by the shifting of curves to the left in the upper plot of Figure 5, and result in larger aggregates (bottom part of Figure 5). Such differences become more pronounced as the friction coefficient decreases, especially when γ is smaller than 1.0. Note that the comparison we made for simulations with different friction coefficient is for the same "physical time", so the larger the friction coefficient, the more simulation steps we need to use. That means within the specified "physical time" the simulation with larger friction coefficient has much longer computer time to evolve the structural quantities and thus get closer to equilibrium as compared to the simulation with smaller friction coefficient. At equilibrium, structural quantities should not depend on the friction coefficients since the use of different friction coefficients should not alter the stationary solution to the Langevin equation, which is the canonical ensemble distribution.

This suggests that simulations with smaller friction coefficients actually slow down the assembly kinetics (since now smaller quenching rates and longer quenching time need to be used to assemble an aggregate of the same size as the one formed in the simulation using larger friction coefficient), and the assembly time estimated from such simulations will be overestimated as compared to the real micellization time. The assembly time estimated in simulations with small friction coefficients is an upper bound of the actual assembly time. Also, because of the highly accelerated nature of our simulated kinetics, the simulated quantities are probably only qualitatively correct. As such, the actual characteristic aggregation time for PS_{1000}−PEO_{3000} at simulation conditions should be even smaller than 6 ms at a polymer concentration of 0.1 wt %. Here we conclude that $\gamma = 1$ is the smallest friction coefficient we can use without significantly altering assembly kinetics, and when $\gamma > 1$, assembly kinetics show a reasonably linear scaling with inverse friction coefficients.

Next we examine an extreme case. Figure 6 shows the assembly trajectories from simulations employing $\gamma = 1$ and $\gamma = 165$. The latter simulation has a time unit of 0.02 ns, consistent with the intrinsic time unit, $\tau_0 = \sigma(m/\varepsilon)^{1/2}$. The effective quenching rate for both simulations was set to be identical, 1881 K/ms in real units. If the simple linear scaling relation between assembly kinetics and inverse friction coefficient still holds, we should observe the same assembly kinetics for the two systems. Even after averaging over five independent simulations, the data are still noisy, especially at the beginning of the simulation, but the time evolution trajectories of the number of aggregates from the two systems are indistinguishable within each other's standard deviations. As was also observed in Figure 5, the simulation with larger friction coefficient tends to form larger final aggregates, but the two trajectories are still within each other's statistical deviation for the size of the largest

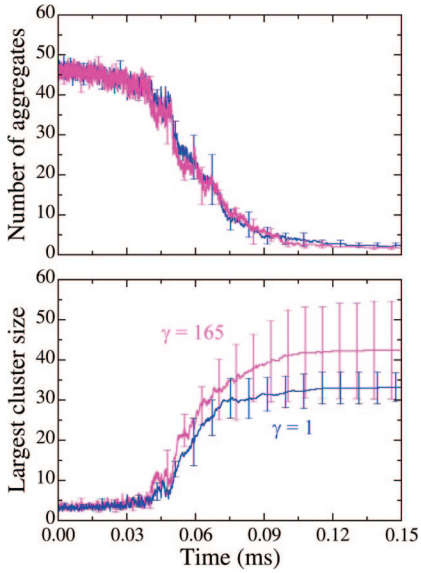

Figure 6. Number of aggregates (upper plot) and size of the largest aggregate (lower plot) as a function of simulation time for a smaller system ($N = 55$, $L = 15$) at a quenching rate of 1881 K/ms, corresponding to a total quenching time of 0.1386 ms. Data are averaged over five independent runs, and standard deviations are shown every 160 (for system with $\gamma = 1$) and 510 data points (for system with $\gamma = 165$) for clarity.

aggregate. This lends us further confidence that we can use a friction coefficient as small as $\gamma = 1$ without significantly altering the assembly kinetics, while gaining a 2 orders of magnitude speed-up.

As far as simulating kinetics is concerned, there is certainly a tradeoff between using explicit (coarse-grained) solvent molecules or implicit solvent as we have done here. Clearly, explicit solvent is necessary to reproduce the correct scaling of diffusivity as a function of polymer molecular weight. On the other hand, an explicit solvent model reduces the time scale a CG simulation can access. When using an implicit solvent model, a smaller friction coefficient in Brownian dynamics simulations can provide extra speed-up of CG simulations. In Kindt et al.'s work on polyethylene melts,[12] they only investigated cases with a moderate speed-up, about 4−32 times by using a smaller background friction coefficient and/or a larger time step. Their study showed no significant deviation in scaled homogeneous kinetics (i.e., no micellization) for the range of small friction coefficients they used. The influence of entanglement in their study does not exist in this work since our system only contains short chains, which can also be verified by our Rouse dynamics. However, the situation studied in the present work is much more complicated due to the micellization occurring during the quenching protocol (gradually changing the solvent quality). Our study clearly demonstrates that when the friction coefficient is too small, the assembly kinetics start to show significant deviation and do not follow the simple linear relationship with inverse friction coefficient when the equilibrium is not reached.

5. Conclusions

In summary, we developed a coarse-grained model for PS−PEO diblock copolymers in aqueous solutions based on pertinent experimental thermodynamic properties using Monte Carlo and histogram reweighting grand canonical Monte Carlo methods. Mesoscale Brownian dynamics simulations were then performed to investigate the rapid assembly of PS−PEO in water on a millisecond time scale. The simulated assembly kinetics is greatly accelerated by coarse-graining several monomers into one CG bead and by the use of implicit solvent with a small friction coefficient. We find that the assembled structures are kinetically frozen when the system is cooled fast and are close to equilibrium when the quenching rate is slow enough (i.e., the rate of solvent quality change is small enough). In addition to the effect of quenching rate, we also investigated the influence of polymer concentration on the assembly kinetics. We found with the current CG model that the average aggregation number, though close to the experimentally measured value, first increases and then decreases as the polymer concentration increases. We investigated the influence of friction coefficient on the assembly kinetics and found that when the friction coefficient is larger than 1, assembly kinetics show a reasonably linear scaling with the inverse friction coefficient. This suggests that we can use a friction coefficient as low as 1 to achieve better computational efficiency while not significantly altering the simulated assembly kinetics. Meanwhile, the assembly time estimated in our CG simulations can at least serve as an upper bound for the characteristic micellization time for the assembly of PS−PEO in water.

We find that within a few milliseconds (up to 3−6 ms), all simulations are able to form clusters with sizes that are comparable to equilibrium micelles of PS_{1000}−PEO_{3000} copolymers. Previous flash nanoprecipitation experimental results showed that polymer nanoparticle size decreased upon decreasing mixing time. When the mixing time is smaller than a characteristic time, the polymer nanoparticle size becomes independent of the mixing rate for mixing times as low as 3 ms. In contrast, polymer micelle size in the simulation increases upon increasing mixing time until after a certain characteristic time (3−6 ms) the size becomes independent of the mixing rate. The polymer nanoparticle (micelle) sizes that are independent of mixing times in simulations and experiments are just the size of the equilibrium micelle of PS_{1000}−PEO_{3000}, ∼ 25 nm or an aggregation number of 41. Since the upper limit of simulation time scale is comparable with the lower limit of experimental time scale, a direct comparison of aggregate sizes on other mixing times between simulations and experiments is not possible. We argue that previous experimental observations probed the formation of micellar clusters between PS−PEO micelles while simulations in this work studied the kinetics of a single PS−PEO micelle assembled from free polymer chains. This work thus provides a microscopic point of view on the assembly mechanism of PS−PEO in aqueous solution and helps better understand the flash nanoprecipitation process.

Although we focused only on one specific block copolymer system here, namely PS_{1000}−PEO_{3000}, the modeling and simulation approach described in this work can be easily extended to study the assembly of other diblock copolymers like poly(ε-caprolactone)-*b*-poly(ethylene oxide),[58,59] also used in the flash nanoprecipitation processes.[3]

Acknowledgment. This work was supported by National Science Foundation Grant NIRT CBET-0506966.

References and Notes

(1) Johnson, B. K.; Prud'homme, R. K. *Phys. Rev. Lett.* **2003**, *91*, 118302.

(2) Johnson, B. K.; Prud'homme, R. K. *Aust. J. Chem.* **2003**, *56*, 1021.

(3) Gindy, M. E.; Panagiotopoulos, A. Z.; Prud'homme, R. K. *Langmuir* **2008**, *24*, 83.

(4) Kong, G.; Braun, R. D.; Dewhirst, M. W. *Cancer Res.* **2000**, *60*, 4440.

(5) Zhu, Z. X.; Anacker, J. L.; Ji, S. X.; Hoye, T. R.; Macosko, C. W.; Prud'homme, R. K. *Langmuir* **2007**, *23*, 10499.
(6) Nielsen, S. O.; Lopez, C. F.; Srinivas, G.; Klein, M. L. *J. Phys.: Condens. Matter* **2004**, *16*, R481.
(7) Srinivas, G.; Discher, D. E.; Klein, M. L. *Nat. Mater.* **2004**, *3*, 638.
(8) Izvekov, S.; Voth, G. A. *J. Chem. Phys.* **2005**, *123*, 134105.
(9) Izvekov, S.; Voth, G. A. *J. Phys. Chem. B* **2005**, *109*, 2469.
(10) Panagiotopoulos, A. Z.; Floriano, M. A.; Kumar, S. K. *Langmuir* **2002**, *18*, 2940.
(11) Padding, J. T.; Briels, W. J. *J. Chem. Phys.* **2002**, *117*, 925.
(12) Kindt, P.; Briels, W. J. *J. Chem. Phys.* **2005**, *123*, 224903.
(13) Espanol, P.; Warren, P. *Europhys. Lett.* **1995**, *30*, 191.
(14) Groot, R. D.; Warren, P. B. *J. Chem. Phys.* **1997**, *107*, 4423.
(15) Usta, O. B.; Ladd, A. J. C.; Butler, J. E. *J. Chem. Phys.* **2005**, *122*, 094902.
(16) Malevanets, A.; Kapral, R. *J. Chem. Phys.* **1999**, *110*, 8605.
(17) Mussawisade, K.; Ripoll, M.; Winkler, R. G.; Gompper, G. *J. Chem. Phys.* **2005**, *123*, 144905.
(18) Depa, P. K.; Maranas, J. K. *J. Chem. Phys.* **2007**, *126*, 054903.
(19) Whitehead, L.; Edge, C. M.; Essex, J. W. *J. Comput. Chem.* **2001**, *22*, 1622.
(20) McGreevy, R. L.; Pusztai, L. *Mol. Simul.* **1988**, *1*, 359.
(21) Lyubartsev, A. P.; Laaksonen, A. *Phys. Rev. E* **1995**, *52*, 3730.
(22) Reith, D.; Putz, M.; Muller-Plathe, F. *J. Comput. Chem.* **2003**, *24*, 1624.
(23) Srinivas, G.; Shelley, J. C.; Nielsen, S. O.; Discher, D. E.; Klein, M. L. *J. Phys. Chem. B* **2004**, *108*, 8153.
(24) Noid, W. G.; Chu, J. W.; Ayton, G. S.; Krishna, V.; Izvekov, S.; Voth, G. A.; Das, A.; Andersen, H. C. *J. Chem. Phys.* **2008**, *128*, 244114.
(25) Noid, W. G.; Liu, P.; Wang, Y.; Chu, J. W.; Ayton, G. S.; Izvekov, S.; Andersen, H. C.; Voth, G. A. *J. Chem. Phys.* **2008**, *128*, 244115.
(26) Bronstein, L. M.; Chernyshov, D. M.; Timofeeva, G. I.; Dubrovina, L. V.; Valetsky, P. M.; Khokhlov, A. R. *Langmuir* **1999**, *15*, 6195.
(27) Mortensen, K.; Brown, W.; Almdal, K.; Alami, E.; Jada, A. *Langmuir* **1997**, *13*, 3635.
(28) Johnson, B. K.; Prud'homme, R. K. *AIChE J.* **2003**, *49*, 2264.
(29) Zimm, B. H. *J. Chem. Phys.* **1956**, *24*, 269.
(30) Rouse, P. E. *J. Chem. Phys.* **1953**, *21*, 1272.
(31) Siepmann, J. I. *Mol. Phys.* **1990**, *70*, 1145.
(32) Ferrenberg, A. M.; Swendsen, R. H. *Phys. Rev. Lett.* **1989**, *63*, 1195.
(33) Ferrenberg, A. M.; Swendsen, R. H. *Phys. Rev. Lett.* **1988**, *61*, 2635.
(34) Floriano, M. A.; Caponetti, E.; Panagiotopoulos, A. Z. *Langmuir* **1999**, *15*, 3143.
(35) Plimpton, S. *J. Comput. Phys.* **1995**, *117*, 1.
(36) Grest, G. S.; Lacasse, M. D.; Kremer, K.; Gupta, A. M. *J. Chem. Phys.* **1996**, *105*, 10583.
(37) Padding, J. T.; Louis, A. A. *Phys. Rev. E* **2006**, *74*, 031402.
(38) Flyvbjerg, H.; Petersen, H. G. *J. Chem. Phys.* **1989**, *91*, 461.
(39) Smith, G. D.; Bedrov, D.; Borodin, O. *Phys. Rev. Lett.* **2000**, *85*, 5583.
(40) Smith, G. D.; Bedrov, D.; Borodin, O. *J. Am. Chem. Soc.* **2000**, *122*, 9548.
(41) Engkvist, O.; Karlstrom, G. *J. Phys. Chem. B* **1997**, *101*, 1631.
(42) Bedrov, D.; Ayyagari, C.; Smith, G. D. *J. Chem. Theory Comput.* **2006**, *2*, 598.
(43) Anderson, J. A.; Lorenz, C. D.; Travesset, A. *J. Chem. Phys.* **2008**, 128.
(44) Polik, W. F.; Burchard, W. *Macromolecules* **1983**, *16*, 978.
(45) Kawaguchi, S.; Imai, G.; Suzuki, J.; Miyahara, A.; Kitano, T. *Polymer* **1997**, *38*, 2885.
(46) Bloustine, J.; Berejnov, V.; Fraden, S. *Biophys. J.* **2003**, *85*, 2619.
(47) Rubinstein, M.; Colby, R. H. *Polymer Physics*, 1st ed.; Oxford University Press: New York, 2003.
(48) Yethiraj, A.; Honnell, K. G.; Hall, C. K. *Macromolecules* **1992**, *25*, 3979.
(49) Dautenhahn, J.; Hall, C. K. *Macromolecules* **1994**, *27*, 5399.
(50) Xiao, C.; Heyes, D. M. *Phys. Rev. E* **1999**, *60*, 5757.
(51) Johnson, B. K. Flash nanoprecipitation of organic actives via confined micromixing and block copolymer statilization. Ph.D. dissertation, Princeton University, 2003.
(52) Torquato, S.; Truskett, T. M.; Debenedetti, P. G. *Phys. Rev. Lett.* **2000**, *84*, 2064.
(53) Frenkel, D.; Smit, B. *Understanding Molecular Simulation*; Academic Press: San Diego, 2001.
(54) Waggoner, R. A.; Blum, F. D.; Lang, J. C. *Macromolecules* **1995**, *28*, 2658.
(55) Shimada, K.; Kato, H.; Saito, T.; Matsuyama, S.; Kinugasa, S. *J. Chem. Phys.* **2005**, *122*, 244914.
(56) Nielsen, S. O.; Lopez, C. F.; Srinivas, G.; Klein, M. L. *J. Chem. Phys.* **2003**, *119*, 7043.
(57) Doi, M.; Edwards, S. F. *The Theory of Polymer Dynamics*; Oxford University Press: Oxford, 1986.
(58) Vangeyte, P.; Gautier, S.; Jerome, R. *Colliods Surf., A* **2004**, *242*, 203.
(59) Vangeyte, P.; Leyh, B.; Heinrich, M.; Grandjean, J.; Bourgaux, C.; Jerome, R. *Langmuir* **2004**, *20*, 8442.

JP805826A